Selection of a Convolution Function for Fourier Inversion Using Gridding

John I. Jackson, Craig H. Meyer, Dwight G. Nishimura, *Member, IEEE,* and Albert Macovski, *Fellow, IEEE*

***Abstract*—In fields ranging from radio astronomy to magnetic resonance imaging, Fourier inversion of data not falling on a Cartesian grid has been a problem. As a result, multiple algorithms have been created for reconstructing images from nonuniform frequency samples. In the technique known as gridding, the data samples are weighted for sampling density and convolved with a finite kernel, then resampled on a grid preparatory to a fast Fourier transform. This paper compares the utility of several convolution functions, including one that outperforms the "optimal" prolate spheroidal wave function in some situations.**

I. Introduction

IN FIELDS ranging from radio astronomy to computerized tomography and magnetic resonance imaging, spatial frequency data is used to generate images. In order to take advantage of the great computational speed afforded by the fast Fourier transform [1], the data must lie on a Cartesian grid. However, because of hardware constraints or practical considerations, this is not always feasible. Accordingly, many algorithms have been developed for reconstruction from nonuniform samples. Some methods use various interpolation schemes, such as nearest-neighbor, bilinear interpolation, and truncated sinc function finite impulse response interpolators [2]–[4]. Other techniques include gradient descent methods [5], or reconstruction using coordinate transformation [6]. For data on a polar grid, such as may be encountered in computerized tomography or diffraction tomography, filtered back-projection [7] may be used for reconstruction.

In this paper we consider the algorithm known as "gridding." In its earliest form, as first used by radio astronomers, the spatial frequency plane was divided into a grid, and the point in the center of each "cell" was then assigned a value equal to the sum of all of the data points falling within the grid [8]. Later improvements included the use of the average value of the data within the cell [9], or weighting the sampling points based on the distance from array points, such as with a Gaussian function [10]. To account for variations in the spectral sampling density, a further modification of the Gaussian weighting method normalizes the sum of the coefficients to be applied to the sampling points to unity. These cell summing, cell averaging, and Gaussian methods have been compared by Thompson and Bracewell [11].

An overview of the gridding operation is given by O'Sullivan [12], who shows that the optimal gridding method is convolution with a sinc ($\sin \pi x/\pi x$) function of infinite extent, followed by sampling onto a Cartesian grid. Practical considerations require that the infinite sinc function be replaced with a finite convolving function. This paper compares the artifact introduced into the image for various convolving functions of different sizes, including the Kaiser–Bessel window and the zero-order prolate spheroidal wave function (PSWF). We also show a convolving function that improves upon the PSWF in some circumstances.

II. Gridding Algorithm

Consider a two-dimensional function $m(x, y)$ with Fourier transform $M(u, v)$ given by

$$M(u, v) = \int_{-\infty}^{\infty} m(x, y) \exp\left[-2\pi i(ux + vy)\right] dx\, dy, \tag{1}$$

and a sampling function S consisting of P two-dimensional delta functions at positions u_j, v_j,

$$S(u, v) = \sum_{j=1}^{P} {}^2\delta(u - u_j, v - v_j). \tag{2}$$

The sampled Fourier data is given by

$$M_S(u, v) = M(u, v) \cdot S(u, v). \tag{3}$$

In gridding, the sampled data is convolved with a function $C(u, v)$ [such as a Gaussian, a sinc, or a small finite window] and sampled onto a unit spaced grid,

$$\begin{aligned} M_{SCS}(u, v) &= [M_S(u, v) * C(u, v)] \cdot \text{Ш}(u, v) \\ &= \{[M \cdot S] * C\} \cdot \text{Ш} \end{aligned} \tag{4}$$

where $*$ denotes two-dimensional convolution, and the shah or comb function $\text{Ш}(u, v)$ is defined as a sum of equally spaced two-dimensional delta functions:

$$\text{Ш}(u, v) = \sum_i \sum_j {}^2\delta(u - i, v - j). \tag{5}$$

Manuscript received November 16, 1990; revised May 8, 1991. This work was supported by the GE Medical Systems Group; the National Institutes of Health under Grants HL-34962, HL-39478, and HL-39297; and the National Cancer Institute under Grants CA 50948 and CA 48269.

The authors are with the Magnetic Resonance Systems Research Laboratory, Stanford University, Stanford, CA 94305.

IEEE Log Number 9102132.

The corresponding reconstructed image m_{SCS} is given by the inverse Fourier transform of M_{SCS},

$$m_{SCS}(x, y) = \{[m(x, y) * s(x, y)] \cdot c(x, y)\} * \text{Ш}(x, y). \tag{6}$$

Here we can observe the effect of $S(u, v)$ on the reconstructed image. First, the inverse Fourier transform of the original sampling function $S(u, v)$, which we refer to as $s(x, y)$, affects the aliasing of $m(x, y)$ at a level that cannot be recovered. Thus, as expected, if the function $M(u, v)$ is not sufficiently sampled, the aliasing cannot be corrected via postprocessing. We can, however, make a correction for a nonuniform sampling density in $S(u, v)$ by introducing an *area density function* $\rho(u, v)$. By defining

$$\rho(u, v) = S(u, v) * C(u, v), \tag{7}$$

areas that are oversampled will have a large area density, while areas that are undersampled will have a small area density. As discussed by Bracewell and Thompson [13], the *principal transfer function* (PTF) is given by $S(u, v)/\rho(u, v)$, and the *principal response pattern* by the two-dimensional Fourier transform of the PTF. Introducing the area density function into the reconstruction, we generate the sampled, weighted, convolved, and sampled M,

$$M_{SWCS}(u, v) = \left\{\left[\frac{M_S(u, v)}{\rho(u, v)}\right] * C(u, v)\right\} \cdot \text{Ш}(u, v),$$

$$= \left(\left\{M \cdot \left[\frac{S}{S * C}\right]\right\} * C\right) \cdot \text{Ш}. \tag{8}$$

Note that the weighted and convolved M_S can be considered a moving weighted average where the sum of the weighting coefficients as determined by $C(u, v)$ has been normalized to one. The corresponding image is given by

$$m_{SWCS}(x, y) = (\{m(x, y) * [s *^{-1} (s \cdot c)]\} \cdot c) * \text{Ш} \tag{9}$$

where $*^{-1}$ refers to a deconvolution.

We now consider the effect of $C(u, v)$ on the reconstructed image. As noted by O'Sullivan [12], the optimal convolution function is an infinite sinc, but this function is computationally impractical. A finite convolving function will contribute sidelobes, which will be aliased back into the image by the shah function. Also, any rolloff in the central lobe of $c(x, y)$ will show up as an attenuation towards the sides of the image. This rolloff can be corrected by dividing by $c(x, y)$. This flattens the response across the central lobe, but amplifies the effective amplitude of the aliasing sidelobes, as shown in Fig. 1 for a Hamming window. As is usually done, we will also limit the image to a finite region of interest containing only one "replication" of the object. This is represented mathematically by multiplying by a two-dimensional rect or boxcar function ${}^2\sqcap(x, y)$ where

$${}^2\sqcap(x, y) = \begin{cases} 1 & \text{if } |x| < 0.5 \text{ and } |y| < 0.5 \\ 0 & \text{otherwise} \end{cases}. \tag{10}$$

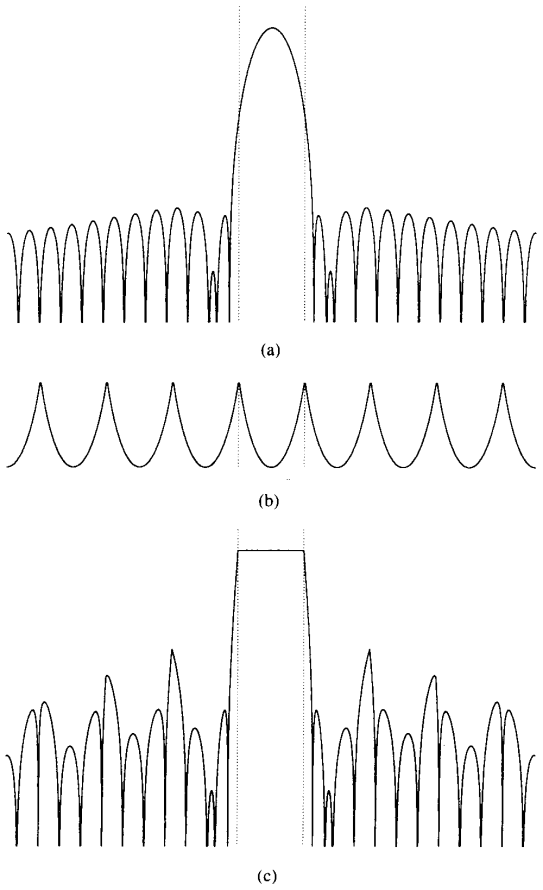

Fig. 1. (a) The log-scale inverse Fourier transform of a Hamming window. The dotted lines represent the edges of the image, with energy in the inverse Fourier transform outside of the dotted lines aliasing back into the image. (b) The convolution rolloff correction for the image. (c) The effective inverse Fourier transform after multiplying by the rolloff correction.

We call the generated image m^*,

$$m^*(x, y) = m_{SWCS} \cdot \frac{{}^2\sqcap(x, y)}{c(x, y)}$$

$$= [(\{m(x, y) * [s *^{-1} (s \cdot c)]\} \cdot c) * \text{Ш}] \cdot \frac{{}^2\sqcap}{c}, \tag{11}$$

and we refer to the method of generating this image as the *gridding algorithm.* The process is illustrated in Fig. 2.

III. Convolution Function Comparison

The utility of any convolution function is determined by the amplitude and placement of the aliasing sidelobes *after* the image has been corrected for rolloff near the edges. For example, gridding using a $\sqcap(x)$ function will suffer from large aliased sidelobes in the image, but none of the sidelobes will alias into the center of the image. If

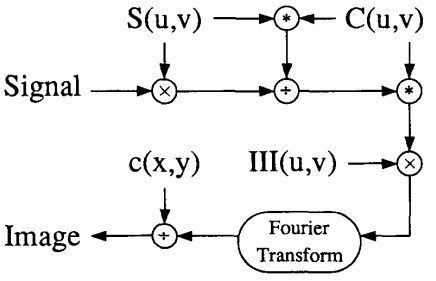

Fig. 2. The gridding algorithm. The signal is sampled by a function $S(u, v)$. The resulting data samples are convolved by the function $C(u, v)$, which is also used to generate the area sampling density weighting. The convolved data are sampled onto a Cartesian grid by multiplying by $\mathrm{III}(u, v)$. Finally, the inverse Fourier transformed data are divided by $c(x, y)$ to compensate for rolloff in the inverse Fourier transform of $C(u, v)$.

the inverse Fourier transform of the convolution function rolls off too much within the bounds of the image, the aliasing into the sides of the image will be greatly amplified when the rolloff is compensated.

We will compare one-dimensional inverse Fourier transforms from separable functions, so $C(u, v) = C(u)C(v)$, and $c(x, y) = c(x)c(y)$. For convenience in working with scale factors, we define the width of the desired image to be 1 unit. The inverse of this, 1 unit of spatial frequency, is the spacing between sampling points in the shah function.

The performance measure that we will use is the relative amount of aliasing energy, including the effect of the rolloff correction. The corresponding functional to be minimized is

$$J = \frac{\int_{|x|>0.5} \left| c(x) \cdot \left[\frac{\sqcap(x)}{c(x)} * \mathrm{III}(x) \right] \right|^2 dx}{\int_{-\infty}^{\infty} \left| c(x) \cdot \left[\frac{\sqcap(x)}{c(x)} * \mathrm{III}(x) \right] \right|^2 dx}, \quad (12)$$

and this is the measure that we will use for comparison.

If all regions within the image are not of equal interest, the performance measure can include a spatially varying weight function, such as Schwab's $w(x, y) = [1 - (2x)^2]^\alpha[1 - (2y)^2]^\alpha$ (where α is a design parameter) [14], which is included in the functional

$$R = \frac{\iint_A |c(x, y)|^2 w(x, y)\, dx\, dy}{\int_{-\infty}^{\infty}\int_{-\infty}^{\infty} |c(x, y)|^2 w(x, y)\, dx\, dy} \quad (13)$$

where A is the region of interest. Our equation (12) is similar to (13) where all regions within the image are of equal interest (so $w(x, y) = 1$), except that (12) includes the rolloff correction effect on the image, and we are considering separable convolving functions, which simplifies the problem to one dimension.

We will consider the following convolving functions:

1) two-term cosine,

$$\alpha + (1 - \alpha) \cos\left(\frac{2\pi}{W} u\right),$$

2) three-term cosine,

$$\alpha + \beta \cos\left(\frac{2\pi}{W} u\right) + (1 - \alpha - \beta) \cos\left(\frac{4\pi}{W} u\right),$$

3) Gaussian,

$$\exp\left[-\frac{1}{2}\left(\frac{u}{\sigma}\right)^2 \right],$$

4) Kaiser–Bessel,

$$\frac{1}{W} I_0[\beta\sqrt{1 - (2u/W)^2}], \text{ and}$$

5) prolate spheroidal wave function, see [15]–[17].

All functions are defined over $|u| \le W/2$, giving each a width W, with α, β, and σ as free design parameters. The well-known Hamming and Hanning windows are examples of the two-term cosine function (with $\alpha = 0.54$ and $\alpha = 0.50$, respectively), and the Blackman window is an example of the three-term cosine function (with $\alpha = 0.42$ and $\beta = 0.50$) [18]. For a given window width and desired bandwidth B the truncated zero-order PSWF of the first kind contains the least amount of energy outside of the desired passband, i.e., it minimizes

$$\frac{\int_{|x|>B} |c(x)|^2\, dx}{\int_{-\infty}^{\infty} |c(x)|^2\, dx}. \quad (14)$$

The PSWF is quite difficult to compute, but the Kaiser–Bessel function [19] is a good approximation, and both it and its inverse transform are easily calculated. The function itself is based on I_0, the zero-order modified Bessel function of the first kind, and the inverse transform is given by

$$c(x) = \frac{\sin\sqrt{\pi^2W^2x^2 - \beta^2}}{\sqrt{\pi^2W^2x^2 - \beta^2}} \quad (15)$$

For each of the functions, the parameters α, β, and σ were varied to determine the best possible performance, as measured by J in (12), at each function width. The resulting values of J are shown in Fig. 3 for the parameter values given in Table I. The relatively poor results are because of the difficulty in generating a finite function whose inverse Fourier transform goes immediately from a near unity passband to a very low amplitude stopband, without allowing for a transition band. The consequence is relatively large errors from the aliasing sidelobes that appear near the edges of the image where the division by $c(x)$, to make the passband uniform, also amplifies the corresponding portions of the sidelobes.

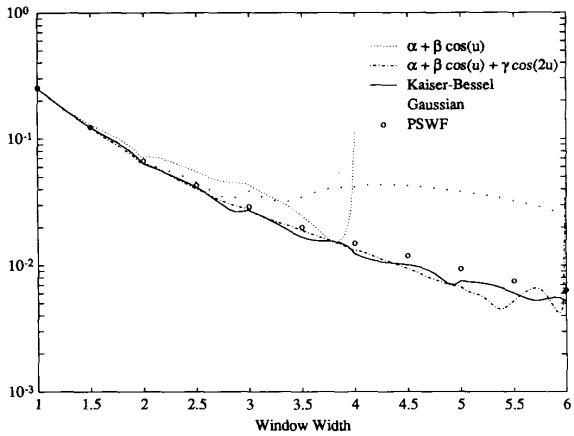

Fig. 3. A comparison of several convolving functions of varying widths, showing the relative amount of unwanted sidelobe energy that will alias into the image if that convolving function is used in the gridding algorithm. Note that when the two-term cosine function reaches a width of four, or when the three-term cosine function reaches a width of six, the first sidelobe of the function's inverse Fourier transform occurs within the image.

TABLE I
THE PARAMETER VALUES FOR EACH FUNCTION TYPE THAT PROVIDE THE LEAST RELATIVE ALIASED ENERGY WHEN GRIDDING ONTO A REGULAR GRID

Window Width	Two-Term cos	Three-Term cos		Gaussian	Kaiser-Bessel
	α	α	β	σ	β
1.5	0.7600	0.8701	0.2311	0.4241	1.9980
2.0	0.7146	0.8099	0.3108	0.4927	2.3934
2.5	0.6185	0.6932	0.4176	0.4839	3.3800
3.0	0.5534	0.5995	0.4675	0.5063	4.2054
3.5	0.5185	0.5383	0.4831	0.5516	4.9107
4.0		0.4998	0.4891	0.5695	5.7567
4.5		0.4653	0.4972	0.5682	6.6291
5.0		0.4463	0.4985	0.5974	7.4302

A simple solution to this problem, alluded to by O'Sullivan [12], is to increase the image field-of-view by sampling onto a smaller grid, and then ignore the outer portion of the image. By doubling the image field-of-view, the central lobe of $c(x)$ can be three times as wide (since it can partially alias around both sides of the image and still not enter the region of interest), which makes possible much smaller amplitude sidelobes [16]. Additionally, $c(x)$ does not taper as much within the region of interest, so less rolloff correction is needed. Conversely, if the former method required Fourier transformation of an $N \times N$ image, subsampling the data in the manner proposed will require transformation of a $2N \times 2N$ image, in addition to computing M_{SWCS} at four times as many points. The computation of M_{SWCS} at each point may be somewhat easier, however, since the subsampling method permits the use of a smaller convolving function for any given error bound.

In addition to the functions previously discussed, we have added a convolving function of our own design. The function was generated in an iterative manner. Starting with any even function, the function was inverse Fourier transformed and those portions of the transformed function that would alias into the region of interest were set to zero. The function was then Fourier transformed back to the original domain and spatially bounded. This process was then repeated many times. This is similar to the method used to generate the PSWF where an even function is repeatedly low-pass filtered and spatially bounded.

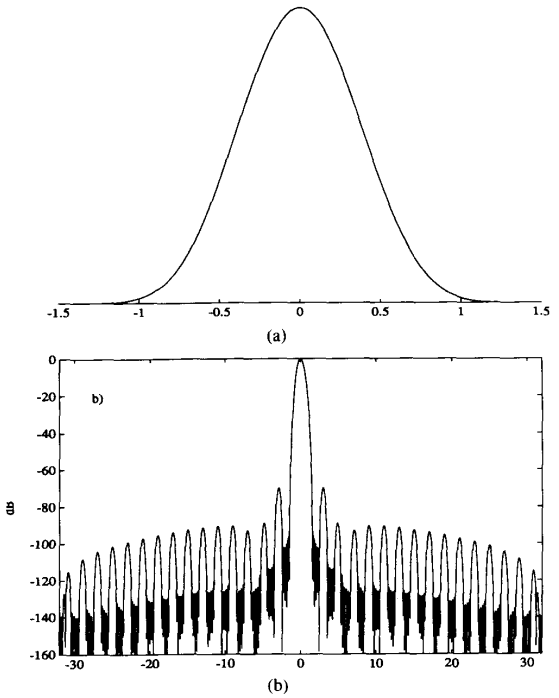

Fig. 4. Authors' width 2.5 convolving function (a) and the corresponding inverse Fourier transform (b). Note the suppression of the portions of the transform that will alias into the center region of the image.

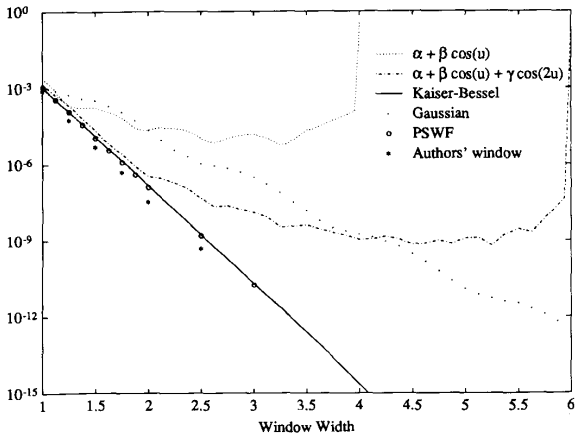

Fig. 5. A comparison of several convolving functions of varying widths, showing the relative amount of unwanted sidelobe energy that will alias into the center region of an image. This center region contains the entire region of interest if the sampled data was gridded onto a 2× subsampled grid.

TABLE II
THE PARAMETER VALUES FOR EACH FUNCTION TYPE THAT PROVIDE THE LEAST RELATIVE ALIASED ENERGY WHEN GRIDDING ONTO A 2× SUBSAMPLED GRID

Window Width	Two-Term cos	Three-Term cos		Gaussian	Kaiser-Bessel
	α	α	β	σ	β
1.5	0.5273	0.4715	0.4917	0.2120	6.6875
2.0	0.5125	0.4149	0.4990	0.2432	9.1375
2.5	0.5076	0.4011	0.4996	0.2691	11.5250
3.0	0.5068	0.3954	0.4997	0.2920	13.9086
3.5	0.5051	0.3897	0.4999	0.3145	16.2734
4.0		0.3850	0.5000	0.3363	18.5547
4.5		0.3833	0.5000	0.3557	
5.0		0.3823	0.5000	0.3737	

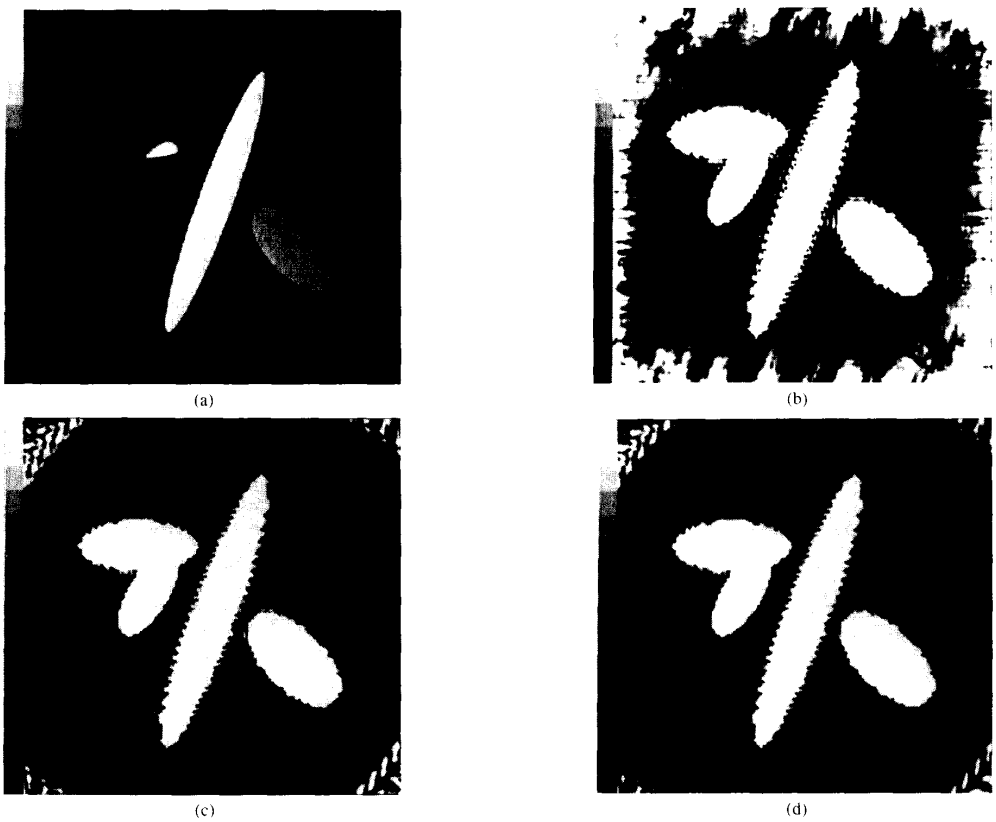

Fig. 6. Reconstructed images of a numerical phantom consisting of four ellipses, showing the effect that the convolution function has on the resulting image. Image (a) was reconstructed using a width three Kaiser-Bessel window ($\beta = 4.2054$), without subsampling. Image (b) is the same as image (a), but scaled from 0 to 5% to show the error in the reconstruction. Image (c) was reconstructed using a width three, two-term cosine window $[0.5068 + 0.4932 \cos(\pi u/1.5)]$ on a subsampled grid, and is scaled the same as image (b). Image (d) was reconstructed using a width three, Kaiser-Bessel window ($\beta = 13.9068$) on a subsampled grid, and is also scaled the same as image (b).

The desired PSWF is the eigenfunction of this operation that has the largest eigenvalue, so all undesired portions of the function will gradually decay away relative to the desired function. In Fig. 4 our width 2.5 function is shown. For wider convolving functions, the sidelobes will be increasingly lower, and many more iterations will be required to generate the function. The function shown is the result after 1 000 000 iterations.

As seen in Fig. 5, the reduction in aliased energy is rather dramatic when the gridding is performed on a subsampled grid. The parameters α, β, and σ for each of the function widths are given in Table II.

Fig. 6 shows the effect that the convolving function has on a reconstructed image. Reconstructions were done using a width three Kaiser–Bessel window on a regular grid, a width three two-term cosine window on a subsampled grid, and a width three Kaiser–Bessel window on a subsampled grid. Improvements in the reconstruction error can be seen with each successive technique.

IV. Conclusion

The gridding algorithm can be implemented with virtually no adverse effects from aliasing sidelobes of the convolving function. This requires that the convolved data is sampled finely enough to yield an image field-of-view that is larger than the actual region of interest. We have found that oversampling by a factor of two in each direction is sufficient to yield excellent sidelobe suppression.

The selection of a convolving function requires two primary considerations. First, the performance of the function, and second, the computation time required to generate the function. Although a (discretized) version of a convolving function needs to be computed only once, this can still be a limiting consideration if the generating computation time is extremely long, as is the case with the PSWF and the authors' function. Only slightly poorer results are achieved with the easily computable Kaiser–Bessel window. Use of the Kaiser–Bessel window requires selecting the free parameter, β. The best choice of β, in the sense of minimizing (12), is given in Table II for several window widths.

References

[1] J. W. Cooley and J. W. Tukey, "An algorithm for the machine calculation of complex Fourier series," *Mathemat. Comput.*, vol. 19, pp. 297–301, 1965.

[2] S. X. Pan and A. C. Kak, "A computational study of reconstruction algorithms for diffraction tomography: Interpolation versus filtered backpropagation," *IEEE Trans. Acoust., Speech, Signal Processing*, vol. ASSP-31, pp. 1262–1275, 1983.

[3] H. Stark, J. W. Woods, I. Paul, and R. Hingorani, "Direct Fourier reconstruction in computer tomography," *IEEE Trans. Acoust., Speech, Signal Processing*, vol. ASSP-29, pp. 237–245, 1981.

[4] H. Stark, J. W. Woods, I. Paul, and R. Hingorani, "An investigation of computerized tomography by direct Fourier inversion and optimum interpolation," *IEEE Trans. Biomed. Eng.*, vol. BME-28, pp. 496–505, 1981.

[5] W. E. L. Grimson, "A computational theory of visual surface interpolation," *Philosoph. Trans. Roy. Soc. London, Series B*, vol. 298, pp. 395–427, 1982.

[6] J. Clark, M. Palmer, and P. Lawrence, "A transformation method for the reconstruction of functions from nonuniformly spaced samples," *IEEE Trans. Acoust., Speech, Signal Processing*, vol. ASSP-33, pp. 1151–1165, 1985.

[7] R. N. Bracewell and A. C. Riddle, "Inversion of fan-beam scans in radio astronomy," *Astrophys. J.*, vol. 150, no. 2, pp. 427–434, 1967.

[8] N. C. Mathur, "A pseudodynamic programming technique for the design ov correlator supersynthesis arrays," *Radio Sci.*, vol. 4, no. 3, pp.235–244, 1969.

[9] D. E. Hogg, G. H. MacDonald, R. G. Conway, and C. M. Wade, "Synthesis of brightness distribution in radio sources," *Astronom. J.*, vol. 74, no. 10, pp. 1206–1213, 1969.

[10] W. N. Brouw, "Aperture synthesis," in *Methods in Computational Physics, Volume 14*, B. Alder, S. Fernbach, and M. Rotenberg, Eds. New York: Academic, 1975, pp. 131–175.

[11] A. R. Thompson and R. N. Bracewell, "Interpolation and Fourier transformation of fringe visibilities," *Astronom. J.*, vol. 79, no. 1, pp. 11–24, 1974.

[12] J. O'Sullivan, "A fast sinc function gridding algorithm for Fourier inversion in computer tomography," *IEEE Trans. Med. Imaging*, vol. MI-4, pp. 200–207, 1985.

[13] R. N. Bracewell and A. R. Thompson, "The main beam and ringlobes of an east-west rotation-synthesis array," *Astrophys. J.*, vol. 182, no. 1, pp. 77–94, 1973.

[14] F. R. Schwab, "Optimal gridding of visibility data in radio interferometry," in *Indirect Imaging*, J. A. Roberts, Ed. New York: Cambridge University Press, 1983.

[15] D. Slepian and H. O. Pollak, "Prolate spheroidal wave functions, Fourier analysis and uncertainty—i," *Bell Syst. Tech. J.*, vol. 40, pp. 43–63, 1961.

[16] H. J. Landau and H. O. Pollak, "Prolate spheroidal wave functions, Fourier analysis and uncertainty—ii," *Bell Syst. Tech. J.*, vol. 40, pp. 65–84, 1961.

[17] D. Slepian, "Prolate spheroidal wave functions, Fourier analysis and uncertainty—iv: Extensions to many dimensions; generalized prolate spheroidal functions," *Bell Syst. Tech. J.*, vol. 43, pp. 3009–3057, 1964.

[18] F. J. Harris, "On the use of windows for harmonic analysis with the discrete Fourier transform," *Proc. IEEE*, vol. 66, pp. 51–83, 1978.

[19] J. F. Kaiser, *Digital filters*, in *System Analysis by Digital Computer*, F. F. Kuo and J. F. Kaiser, Eds. New York: Wiley, 1966, ch. 7.